Feasibility study on temperature control with phase change material in intensive heat-releasing space during emergency power failure: A case analysis of information system room

Jing Wang, Xiaoling Cao *, Yanping Yuan, Ziyu Leng, Yafen Sun

School of Mechanical Engineering, Southwest Jiaotong University, Chengdu 610031, Sichuan, China

ABSTRACT

Phase change material (PCM) is widely used to control temperature because of its easy control, and independent work even without external power supply. However, few studies focus on temperature control via a PCM cooling system without auxiliary facilities, in an intensive heat-releasing space during emergency power failure. This study takes an information system room with an emergency power failure as the research object. A cooling system implementing PCM plates is proposed and its feasibility is analyzed. A mathematical heat transfer model, which considers the air, heat source, phase change cooling devices, and the enclosure structure of room, is established. The performance of the PCM and air temperature are analyzed, and the effects of the melting temperature, latent heat, thermal conductivity, and size of the PCM plates are systematically investigated. Analysis results indicate that: (i) Under the condition of parameter optimization, the air temperature is 32.10 °C at 9 h. Therefore, the cooling system utilizing the PCM plates can effectively maintain the air temperature of the information system room below 35 °C within 9 h. Until 16 h, the air temperature remains below 35 °C. (ii) Increasing the aspect ratio of PCM plates and decreasing PCM latent heat have the similar effect on the air temperature control. Additionally, the two parameters are related to the surface area of the PCM plates. (iii) The lower the melting temperature of the PCM, the better the air temperature can be controlled. For the conditions considered in this study, the appropriate melting temperature is approximately 25 °C. (iv) As thermal conductivity increases, air temperature reduces, and fluctuation of the PCM heat flow significantly decreases. However, as the thermal conductivity approaches 1 W/(m·K), further increases in the thermal conductivity have no marked impact on air temperature control.

© 2020 Published by Elsevier B.V.

1. Introduction

Currently, the information era is developing. Information system rooms, an important part of information transmission, an important part of information transmission, are typical closed spaces with intensive heat-releasing and high temperature control requirements. The relative standards of China require that the temperature of an information system room should be controlled at 5–35 °C when the equipment is not running, and at 22–24 °C when the equipment is running [1]. In the case of a power outage, the air conditioning system will not work properly. However, other equipment in the information system room will continue working, because of an uninterruptible power supply. This leads to a signif-

icant rise in the temperature of the information system room, which can greatly influence the safe operation of the units and other process equipment in the room. Phase change material (PCM) is widely used to control temperature because of its easy control, and independent work even without external power supply. According to phase change energy storage theory, temperature can be controlled as long as the amount of latent heat from the PCM is enough to satisfy the requirement of the cooling load. Therefore, PCM can be used to control the temperature in the information system room.

Many scholars have studied the use of PCM to control temperature. Jin Hou et al. [2] used PCM to reduce thermal stress and improve human thermal comfort in the thermal environment. Taig Young Kim et al. [3] and Adeel Arshad et al. [4] combined PCM with radiators to reduce the temperature of radiators. Wanfan Wu et al. [5] proposed a shape-stabilized PCM with high thermal

---

Nomenclature

A_P	Area, m^2		μ	Dynamic viscosity, Pa/s
A_{mush}	Mushy zone constant		υ	Kinematic viscosity, m^2/s
C	Specific heat, J/(kg·K)		Φ	Heat flow, W
c_p	Constant pressure specific heat, J/(kg·K)			
g	Acceleration of gravity, m/s^2		*Subscript*	
h	Convective heat transfer coefficient, W/(m^2·K)		P	PCM plate
h	Enthalpy, J/kg		a	Air
H	Enthalpy, J/kg		ref	Reference
H	High, mm		x	x Direction
k	Thermal conductivity, W/(m·K)		y	y Direction
K	Heat transfer coefficient,W/(m^2·℃)		S	Solid
l	Feature size, m		l	Liquid
L	Length, m		e	Enclosure structure of information system room
L	Latent heat, kJ/kg		f	Flow air
N	Number		m	Melt
P	Pressure, Pa		efr	External wall, floor or roof
Q	Heat, J		da	Daily average
S	Momentum source term		pc	Position correction
T	Temperature, ℃		i	Inner enclosure
u	Velocity, m/s		ao	Average outdoor temperature
V	Volume, m^3		ar	Adjacent room
v	Velocity, m/s		V	Volume
w	Velocity, m/s			
W	Width, mm		*Abbreviation*	
			CFD	Computational Fluid Dynamics
Greek symbols			PCM	Phase Change Material
α	Expansion coefficient, 1/K		UDF	User Define Function
ε	Constant number			
δ	Thickness, mm		*Dimensionless numbers*	
Δ	Difference		Nu	Nusselt number
Δ	Modification		Pr	Planck number
λ	Liquid fraction		Gr	Grashof number
ρ	Density, kg/m^3			
τ	Time, s			

conductivity to be used on a spacecraft, aiming to address the damage incurred by spacecrafts due to short-term high heat flow. Angelo Maiorino et al. [6] applied PCM to a refrigerator cabinet to reduce the temperature gradient in the refrigerator and the fluctuation of food temperature. It can be seen from these various applications that PCM can play an important role in energy conservation and temperature control. However, in contrast to electronic components and the human body, an information system room without power experiences a large heat release and small temperature differences. Therefore, the effect of temperature control in the information system room via PCM needs to be analyzed.

In the literature on temperature control via PCM, many studies focus on the application of PCM in buildings. Some scholars have combined PCM with building envelopes to reduce indoor air temperature [7–11], for example, with Mushtaq I. Hasan et al. [7] combined PCM with the walls and the ceilings of residential buildings. Other scholars have combined PCM with the cooling or heating system in buildings. M. Alizadeh et al. [12] proposed a new, free cooling and heating approach that combines PCM with ceiling fans. Xiaoming Chen et al. [13] studied the potential application of ventilation systems with thermal energy storage (TES) using PCM for space cooling in air-conditioned office buildings in Beijing during the summer. Sanghoon Baek et al. [14] studied the PCM radiant floor heating system and analyzed its impact on the indoor environment and energy consumption. Chaiyat N et al. [15] proposed adding PCM to the air conditioning system to improve the cooling efficiency of air conditioning.

Our team has conducted research that focuses on environmental temperature control in buildings without auxiliary facilities. Yuan and Cao et al. [16,17] applied a PCM cooling system without auxiliary facilities to control the temperature of the refuge chamber. Numerical results showed that this system can satisfy temperature regulation requirements, according to which the temperature should not exceed 35 °C within 96 h without any external power supply. The temperature of surrounding rock is low and stable, such that the surrounding rock of the refuge chamber can pre-cool the refuge chamber; thus, the surrounding rock is beneficial for temperature control. However, the environment of the information system room is different than the environment of the refuge chamber. The enclosure structure of information system room is affected by the external environment, which increases the indoor load. Additionally, the heat release of the information system room is much larger than that of the refuge chamber, which will have an adverse influence on the effect of temperature control. Therefore, the feasibility and effect of temperature control in an intensive heat-releasing machine room by using a PCM cooling system without auxiliary facilities must be analyzed.

This study takes an information system room with an emergency power failure as the research object. PCM is used to absorb heat and maintain air temperature below 35 °C in a period of 9 h. To avoid the frost caused by the combination of PCM and the envelope of the information system room, PCM plates are placed indoors. The current study aims to demonstrate the feasibility of temperature control in an intensive heat-releasing space by

applying phase change cooling devices that implements PCM plates. Moreover, analyzing the PCM physical parameters for better cooling performance is another purpose of this study. Thereafter, the mathematical heat transfer model, which addresses the air, heat source, phase change cooling devices, and the enclosure structure of room, is established. Moreover, some results are analyzed, such as the liquid fraction of PCM, heat flow of the total PCM plates, and air temperature. Finally, the factors affecting the air temperature change, including the melting temperature, latent heat, thermal conductivity, and size of the PCM plates, are investigated in detail.

2. Physical model and parameters

According to the Chinese standard [1], the temperature of an information system room should be maintained at 5–35 °C when the equipment is not running, and at 22–24 °C when the equipment is running. Therefore, the initial temperature of an information system room is set to 22 °C, with the intent to maintain the temperature of the room below 35 °C within 9 h in the case of an emergency power failure. Here, the geometry size of the information system room is 6.74 m × 6. 2 m × 2.7 m. The total heat load from the equipment in the room is 18 kW. There are 10 sets of racks in the room, divided into two groups. The size of each rack is 1.2 m × 0.75 m × 2 m [18].

There is a large amount of equipment in the room, and the space provided for the PCM is not enough. Additionally, the combination of the PCM and the envelope may cause frost. Therefore, here it is proposed that the PCM plates be placed on brackets, and the brackets placed on the aisle between the equipment. The three-dimensional schematic of the information system room containing the phase change cooling devices is shown in Fig. 1. Moreover, a phase change cooling device consists of the PCM plates and a bracket, as shown in Fig. 2. If the bracket and the PCM plates are in plate contact, only one side of the PCM plate can exchange heat with the air. Thus, to further enhance the convective heat transfer effect between the PCM plate and the indoor air, the bracket adopts the form of parallel bars, such that the back of PCM plates can also be ventilated. The schematic diagram of proposed cooling method is shown in Fig. 3.

The PCM plate is a rectangular box that is encapsulated by a thin metal plate, which is an aluminum plate with a thickness of
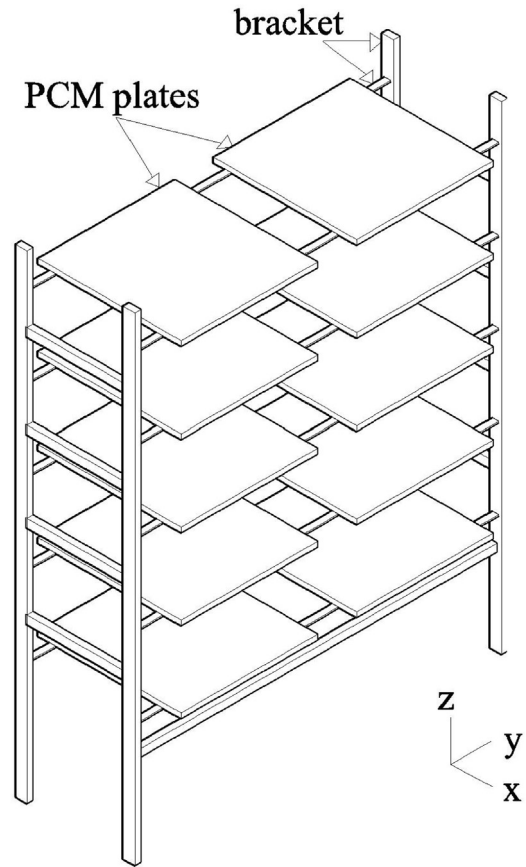

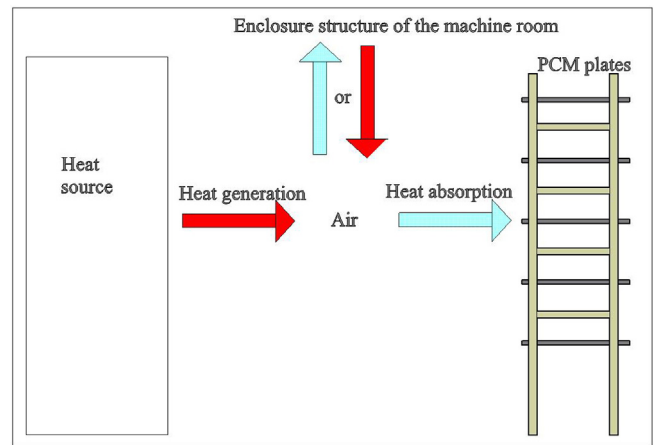**Fig. 2.** Model diagram of the phase change cooling device.

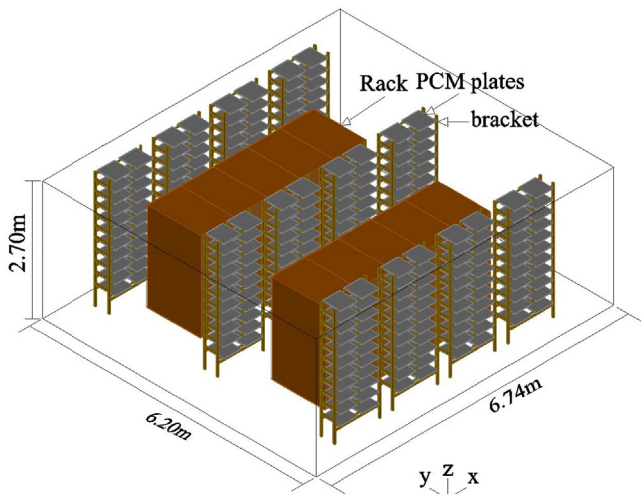**Fig. 3.** Schematic diagram of proposed cooling method.

2 mm, and filled with PCM inside. It can be seen from the literature [19,20] that better performance can be obtained with a longer and thinner PCM plate size. Thus, a PCM plate with a larger aspect ratio is selected here. The dimensions of the PCM plate (excluding aluminum plate) are 600 mm × 500 mm × 50 mm. RT 26 [21] is adopted as the PCM, because of its safe and pollution-free characters, and its melting temperature at room temperature. Further relevant material parameters are shown in Table 1.

A preliminary design of the number of PCM plates can be calculated with the following formula:

$$\Phi_{max} = \Phi + \Phi_{emax} \tag{1}$$

Fig. 1. Three-dimensional schematic of the information system room containing the phase change cooling devices.

Table 1
Thermo-physical properties of RT 26 and aluminum.

Materials	Density (kg/m³)	Thermal conductivity (W/(m·K))	Specific heat capacity (kJ/(kg·K))	Melting temperature range (°C)	Latent heat of fusion (kJ/kg)	Viscosity (kg/(m·s))	Thermal expansion coefficient(1/k)
RT 26	750/880 (Liquid/ Solid)	0.2	2	25–26 main peak:26	180	0.07	5×10^{-4}
Aluminum	2719	202.4	0.87	–	–	–	–

$$Q_{max} = \Phi_{max}\tau \tag{2}$$

$$V_p = Q_{max}/L\rho \tag{3}$$

$$N_p = V_p/V_{plate} \tag{4}$$

where Φ_{max} is the max indoor heat flow, Φ = 18 kW is the heat release of the device, and Φ_{emax} is the max convective heat flow between the air and enclosure structure of information system room; Q_{max} is the max indoor heat; τ is the time; V_p is the volume of PCM; V_{plate} is the volume of a PCM plate; L is the latent heat of the PCM; ρ is the density of PCM; N_P is the number of PCM plates.

According to Eqs. (1)–(4), it is calculated that the max indoor heat flux Φ_{max} is 19.35 kW, and the estimated initial number of PCM plates N_p is 264.

3. Mathematical model

The cooling process includes heat transfer among the phase change cooling devices, enclosure structure, and air and heat sources in the information system room (as shown in Fig. 3). The heat generated by the electronic equipment in the information system room is eventually absorbed by the air, PCM plates, and enclosure structure. The following major assumptions are employed when deducing the control equation:

1) The heat source is constant and the effect of radiation is ignored.
2) The dynamic characteristics of indoor air temperature are studied by the lumped parameter method.
3) It is assumed that the PCM is isotropic, the thermophysical properties of the PCM remain unchanged, the density of the solid phase and liquid phase of the PCM is almost the same, and the influence of density change on buoyancy is only considered when the temperature change of the liquid phase is involved.
4) The temperature gradient change in the length direction of the PCM plate is ignored, and the heat transfer of the PCM plate is simplified to the two-dimensional heat transfer process in the direction of the width and height.
5) The contact area between the PCM plate and the fixed part is ignored.

3.1. Heat transfer of the information system room's enclosure structure

The information system room located in Chengdu has one external wall and three inner walls. The parameters of the envelope structure are shown in Table 2 [22,23]. Here, the most unfavorable condition is selected as the calculation. The heat flow caused by the heat transfer of the external wall, floor, or roof Φ_{efr} can be calculated by Eq. (5) [24]:

$$\Phi_{efr} = KA(T_{da} + \Delta T_{pc} - T_f) \tag{5}$$

where, K is heat transfer coefficient and A is the area of the envelope structure; T_{da} is the daily average of the cold load temperature; ΔT_{pc} is the position correction of the cold load temperature; the indoor air temperature is T_f.

The heat flow between the air and the inner enclosure Φ_i is calculated by Eq. (6) [24]:

$$\Phi_i = KA(T_{ao} + \Delta T_{ar} - T_f) \tag{6}$$

where, T_{ao} is the average outdoor temperature of a typical day in the summer, and ΔT_{ar} is the temperature modification value that depends on the heat dissipation intensity of the adjacent room.

Φ_e, the convective heat flow between the air and enclosure structure of the information system room, can be calculated by the following formula:

$$\Phi_e = \Phi_{efr} + \Phi_i \tag{7}$$

More detailed calculations are available in the literature [24].

3.2. Heat transfer of the phase change device

Assuming uniform air temperature distribution, the heat transfer mathematical model of the phase change device can be simplified as a single PCM plate.

According to the structure and arrangement of the PCM plate, the PCM plate is a flat plate placed horizontally; its length and width are much larger than its height, such that the change of the length direction can be neglected. As shown in Fig. 4, the vertical mid-plane of the PCM plate is selected as the computational domain. There is convective heat transfer between the outside of the PCM plate and the air; the heat conduction, convection, and melting endothermic processes exist inside the PCM plate. T_P is the outer surface temperature of the PCM plate; h_P is the convective heat transfer coefficient; T_f is the air temperature; H_P is the PCM plate height; W_P is the PCM plate width; δ is the aluminum plate thickness.

The phase transition process was solved by using the enthalpy-porous media model proposed by Voller and Prakash [26]. The enthalpy-porous media model is a kind of enthalpy method, which pays attention to the volume occupied by liquid in each cell in the grid, that is, the 'liquid phase fraction'. The mushy zone, which is the region where the phase transition occurs, is considered to change the porosity of the porous material from 0 to 1. The enthalpy-porosity method adds a source term to the momentum equation. When the larger value is taken in the solid phase, the velocity is forced to approach zero [25].
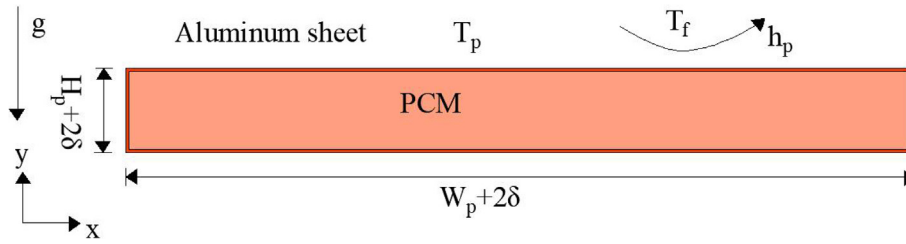
Table 2
Parameters of the envelope structure.

Heat transfer coefficient	External wall	Inner wall	Floor	Ceiling
K (W/(m²·℃))	1.1	2.0	1.2	0.8

Fig. 4. Computational domain and boundary conditions at the vertical mid-plate of the PCM plate.

The continuity equation, the momentum equation, and the energy equation as the governing equation are expressed according to Brent, Voller, and Reid [25] and Voller and Prakash [26].

The continuity equation is expressed as:

$$\frac{\partial(\rho u)}{\partial x} + \frac{\partial(\rho v)}{\partial y} = 0 \qquad (8)$$

The momentum equation is expressed as:

$$\frac{\partial(\rho u)}{\partial t} + \frac{\partial(\rho uu)}{\partial x} + \frac{\partial(\rho uu)}{\partial y} = -\frac{\partial P}{\partial x} + \frac{\partial}{\partial x}\left(\mu \frac{\partial u}{\partial x}\right) + \frac{\partial}{\partial y}\left(\mu \frac{\partial u}{\partial y}\right)$$
$$+ S_x \qquad (9)$$

$$\frac{\partial(\rho v)}{\partial t} + \frac{\partial(\rho uv)}{\partial x} + \frac{\partial(\rho uv)}{\partial y} = -\frac{\partial P}{\partial y} + \frac{\partial}{\partial x}\left(\mu \frac{\partial v}{\partial x}\right) + \frac{\partial}{\partial y}\left(\mu \frac{\partial v}{\partial y}\right)$$
$$+ S_y \qquad (10)$$

The source terms are defined by the karmen-kozeny item as follows:

$$S_x = -\frac{(1-\lambda)^2}{\lambda^3 + \varepsilon} A_{mush} u \qquad (11)$$

$$S_y = -\frac{(1-\lambda)^2}{\lambda^3 + \varepsilon} A_{mush} v \qquad (12)$$

where, ρ is the density of the PCM; u,v are the velocity components along the x,y directions, respectively; μ is the dynamic viscosity of PCM; P is the pressure of the PCM fluid; S_x is the momentum source term in the x direction; S_y is the momentum source term in the y direction; λ is the liquid fraction of the PCM; A_{mush} is the mushy zone constant (10^5), and its value in the range of 10^5-10^6 can predict the experiment more accurately [20,27,28]; ε is a small value to prevent division by zero ($\varepsilon = 0.001$) [29].

The energy equation is expressed as:

$$\frac{\partial}{\partial t}(\rho H) + \frac{\partial}{\partial x}(\rho uH) + \frac{\partial}{\partial y}(\rho vH) = \frac{\partial}{\partial x}\left(k\frac{\partial T}{\partial x}\right) + \frac{\partial}{\partial y}\left(k\frac{\partial T}{\partial y}\right) \qquad (13)$$

where H is the total enthalpy of the PCM and is calculated as the sum of sensible heat enthalpy (h) and latent heat enthalpy (ΔH) [30], as follows:

$$H = h + \Delta H = h + \lambda L = h_{ref} + \int_{T_{ref}}^{T} c_p dT + \lambda L \qquad (14)$$

Here, h_{ref} is the reference enthalpy of the PCM; T_{ref} is the reference temperature; c_p is the constant pressure specific heat; ΔH is the latent heat of the PCM; L is the latent heat capacity of the PCM.

It is assumed that the heat release in the mushy zone is linear, and that the liquid fraction has a linear relationship with the temperature, such that the liquid fraction λ can be defined by Eq. (15):

$$\lambda = \begin{cases} 0, T < T_s \\ \frac{T - T_s}{T_l - T_s}, T_s \leqslant T \leqslant T_l \\ 1, T > T_l \end{cases} \qquad (15)$$

where, T_s, T_l are the solidification and liquefaction temperatures, respectively.

The outer boundary of the PCM plate is set as a natural convection boundary condition, where the convective heat transfer coefficient is h_p, the air temperature is T_f, the temperature value of the outer wall surface of the PCM is T_p, and k_p is the thermal conductivity of the PCM. The boundary conditions are as follows:

$$\begin{cases} -k_P \frac{\partial T}{\partial x} = h_P[T_P - T_f] \\ -k_P \frac{\partial T}{\partial y} = h_P[T_P - T_f] \end{cases} \qquad (16)$$

h_p can be calculated by Eqs. (17) and (18) [31]:

$$Nu = \frac{h_P l}{k_a} \qquad (17)$$

$$Nu = 0.59(GrPr)^{1/4} \qquad (18)$$

where, Nu is the Nusselt number, k_a is the thermal conductivity of air, Pr is the Planck number of air. L is the feature size and the height H is selected as the feature size here [30,32]; theoretical scale analysis shows that height is a physically meaningful choice [33]. Gr is the Grashof number, where g is the acceleration of gravity, α_V is the air volume expansion coefficient, ΔT is the temperature difference, and v is the kinematic viscosity; Gr is calculated as follows [31]:

$$Gr = \frac{g\alpha_V \Delta T l^3}{v^2} \qquad (19)$$

The initial temperature condition of the PCM plate is:

$$T(x,y,0) = 22\ °C \qquad (20)$$

3.3. Heat transfer of indoor air

Using the law of conservation of energy, an equation is established for the heat transfer process of indoor air [16,17]:

$$\Phi_a = C_a \rho_a V_a \frac{\partial T_f}{\partial \tau} = \Phi - \Phi_e - \Phi_P \qquad (21)$$

where, Φ_a is the indoor heat flow; Ca is the specific heat of air; ρ_a is the density of the air; V_a is the volume of air; τ is the time; $\Phi = 18$ kW is the heat release of the device; Φ_e is the convective heat flow between the air and the enclosure structure of the information system room. Because of the constant change of air temperature in the information system room, Φ_e is a positive value when the indoor air temperature is higher than the outdoor temperature, and a negative value when the indoor air temperature is lower than the outdoor temperature [22]. Φ_P, the convective heat flow between the air and PCM plate, can be calculated as follows:

$$\Phi_P = N_P h_P A_P (T_f - T_P) \qquad (22)$$

where, N_P is the number of PCM plates, A_P is the area of the outer surface of a PCM plate, and T_p is the temperature value of the outer wall surface of the PCM plate.

4. Numerical solution method and model validation

4.1. Numerical solution method

The overall model considers the coupling heat transfer of the phase change-cooling devices, the enclosure structure of the information system room, the air, and the indoor heat source. The information system room is much larger than the PCM plate, and complex heat conduction, convection, and melting processes occur inside the PCM plate. If a three-dimensional whole-field numerical model is used to solve the solution, a large number of meshes need to be built for each PCM plate to ensure the accuracy of the calculation. As a result of the above reasons, use of the whole model with three-dimensions makes the number of grids huge, and the calculation difficult. Therefore, ANSYS Fluent is used to simulate the internal heat transfer of the PCM plates. The heat transfer of the outer aluminum surface of the PCM plate is a convection process. The boundary conditions are solved by a user defined function (UDF). The interface between the aluminum surface and the PCM is the coupled interface.

4.1.1. Simulation of the PCM plate

Gambit is used as a meshing tool to mesh the PCM plates. ANSYS Fluent is used as a numerical calculation tool to calculate the change process in the PCM plate. The calculation is based on the melting and solidification model. The density calculation is based on the Boussinesq assumption. Pressure and velocity coupling is conducted using the SIMPLE algorithm. For pressure correction, the PRESTO! scheme is employed. The under relaxation factors are 0.3, 1, 0.7, 0.9, and 1, corresponding to pressure, density, body forces, and momentum, respectively. The scaled absolute residuals of 10^{-4}, 10^{-5} and 10^{-6} are set as the convergence criteria for continuity, momentum, and energy, respectively. The flow is dominated by natural convection, and the flow is laminar [20,32,34]. The heat transfer of the outer surface of the PCM plate is the third type of boundary condition. The time step is 1 s, and the total number of steps is 57,600. The total calculation time is set to 16 h, and each iteration is calculated 20 times.

4.1.2. Calculation of the cooling system

The flow chart of the UDF program is shown in Fig. 5. Since the air temperature T_f is the core of all components, the idea of the cooling system calculation is to calculate the air temperature by using the trial algorithm. The main calculation process is divided into the following steps [16]:

1) Input initial parameters, set $\Phi_a = 0$, and read T_P from Fluent;
2) Set the increment of $\Delta\Phi = 1$ W and calculate $\Phi_a = \Phi_a + \Delta\Phi$;
3) Calculate T_f with Eq. (21), and then calculate h_P with Eqs. (17)–(19). With the calculated T_f, and h_P, the value of Φ_e and Φ_P can also be obtained.
4) Determine the size of $\Phi_a + \Phi_P$ and $\Phi + \Phi_e$. If $\Phi_a + \Phi_P < \Phi + \Phi_e$, which indicates that the air temperature value is less than the real result, then return to the Step (2) and calculate again; if $\Phi_a + \Phi_P \geqq \Phi + \Phi_e$, stop the calculation;
5) Save and output T_f and h_P to Fluent.

4.2. Independence validation of grids and time step

To ensure the accuracy of the numerical simulation, grid and time step independence studies are performed for the PCM plate. Figs. 6 and 7 show the liquid fraction curves during the melting time for different element sizes and time steps, respectively. Fig. 6 shows that when the mesh size is 0.55 mm, the change in the liquid fraction is less than 0.1%. Thus, the 0.55 mm grid size
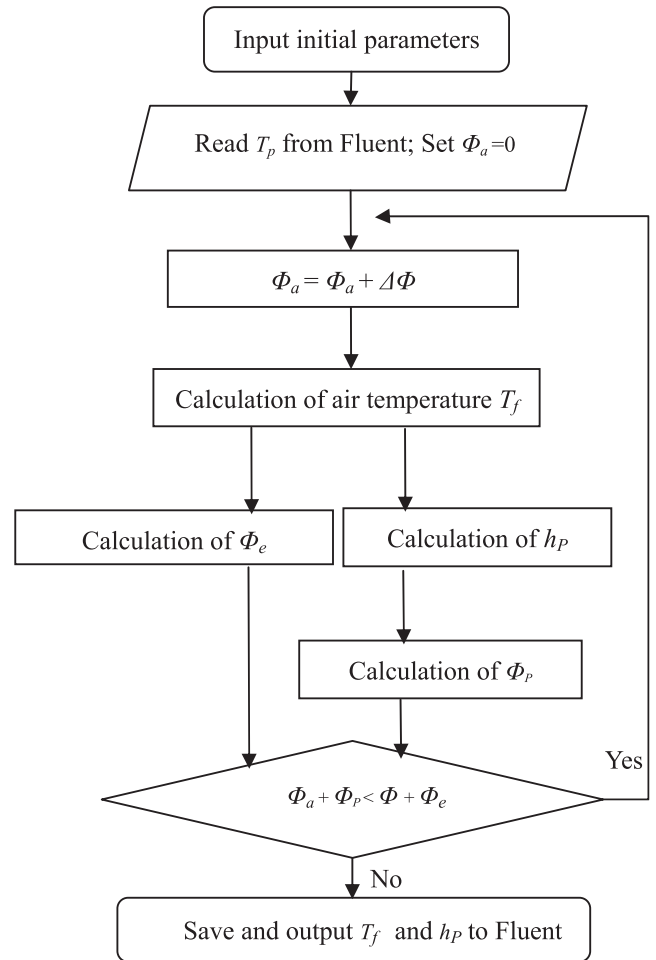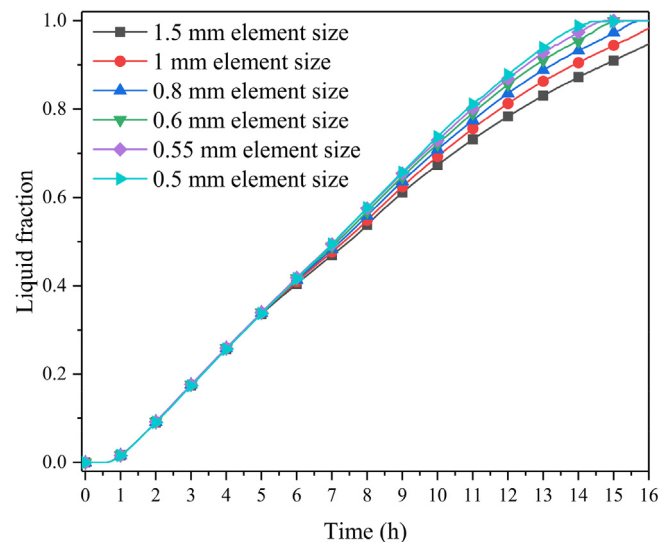

Fig. 5. Flow chart of UDF program.

Fig. 6. Comparison of liquid fraction across different grids.

is selected for calculation. Fig. 7 demonstrates the insignificant effect of the decrease in time step from 1 s to 0.5 s. The time step of 1 s is selected for calculation.
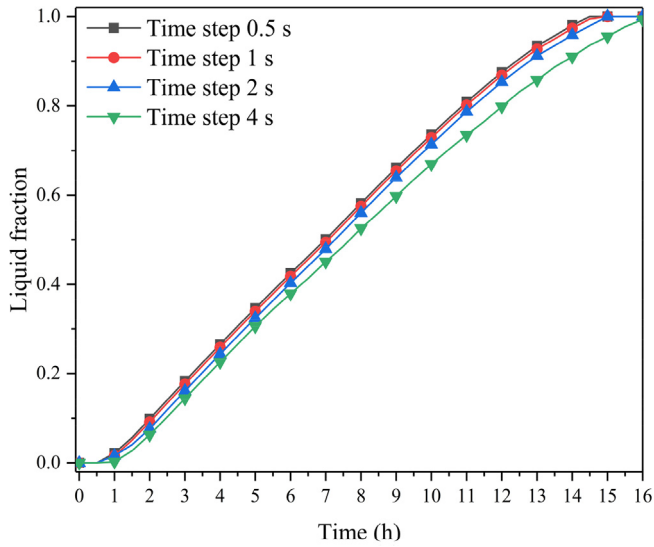
Fig. 7. Comparison of liquid fraction across different time steps.

4.3. Model validation

To verify the numerical model, the simulation results are compared with the experimental data of Wu B et al. [35]. Their experiment was conducted in a rectangular box with a size of 1 m × 0.9 m × 1.2 m, and the outer surface of the box was covered with heat-insulating cotton to prevent heat exchange between the external environment and the experiment box. PCM with a volume of 176 L was encapsulated in the color steel plate, and the color steel plate was then placed in the rectangular box. The temperature inside the chamber was measured with temperature sensors, the experimental time lasted for 96 h, the initial temperature was 15 °C, and the indoor heat source was 170 W. The PCM was a type of crystalline hydrated salts, the melting point was 28 °C, and the latent heat was 360 kJ/L. The specific heat capacity was 1.6 kJ/(kg·K), and the thermal conductivity was 0.6 W/(m·K). Fig. 8 shows a comparison of the temperature changes of the experimental data and the simulated data. Since the PCM has already melted at a lower temperature in the experiment, the error between the experimental and the simulation results is large in the first few hours,
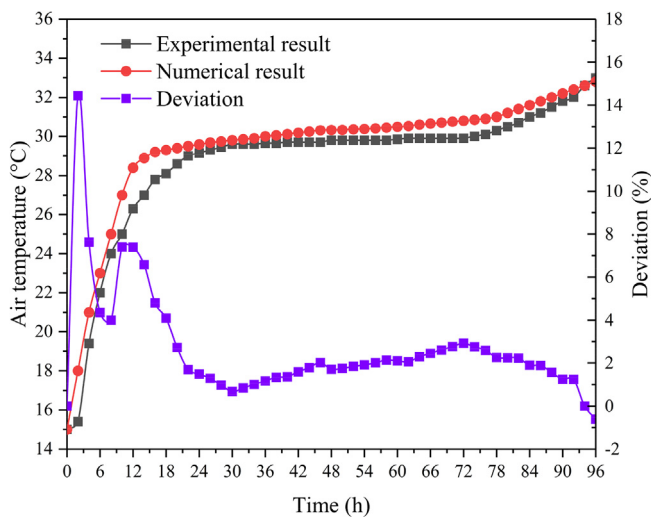
with a maximum deviation of 14.44%. As time elapsed, the error curve flattens when the melting rate of PCM becomes steady, and the errors remain within ± 4%. The high level of agreement between the experimental and simulation results suggest that the mathematical heat transfer model developed in this study is feasible.

5. Results and discussion

Fig. 9 shows the variation of the liquid fraction in the PCM plates over time. It can be seen that the PCM does not melt completely until 14.76 h. The liquid fraction is only 0.66 at 9 h. The reason could be that, in the case of natural convection, the low thermal conductivity of air leads to the slow heat transfer rate of air. However, this point is not taken into account in the theoretical calculation of the relevant parameters of the PCM plate. Therefore, the calculation results are deviated from the theoretical results and the simulation ends at 16 h. The liquid fraction curve shows that the PCM begins to melt at 0.58 h, and the liquid fraction increases almost linearly with time.

Figs. 10 and 11 show the contour distribution of liquid fraction and temperature inside the PCM plate at different times respectively. At the beginning of melting, as shown in Fig. 10 (a) and 11 (a), PCM begins to melt, and the solid–liquid interface is similar to the shape of rectangular container. At this time, PCM's main heat transfer mode is heat conduction and the temperature distribution is uniform. With the increase of time, as shown in Fig. 10 (b) and Fig. 11 (b), PCM near the wall rapidly melts and the mode of heat transfer is transformed from heat conduction to convection. The heated fluid near the wall decreases in density and flows up the wall, leading to a faster melting rate of solid PCM at the top. As the hot liquid occupies the top of the rectangular container, thermal stratification is taking place. Afterwards, as shown in Figs. 10 and 11 (c) and Figs. 10 and 11 (d), PCM continuously absorbs heat, making the amount of liquid PCM ascend. With the enhancement of natural convection to a certain extent, ripples begin to appear in the solid–liquid interface at the bottom. Other scholars have also discovered and explained this phenomenon[30,36,37]. When the time is 15 h, Fig. 10 (e) and Fig. 11 (e) show that solid PCM has been completely melted and the temperature is completely stratified.

Fig. 12 illustrates the variation of air temperature and heat flow of total PCM plates over time. It can be seen that there is a direct
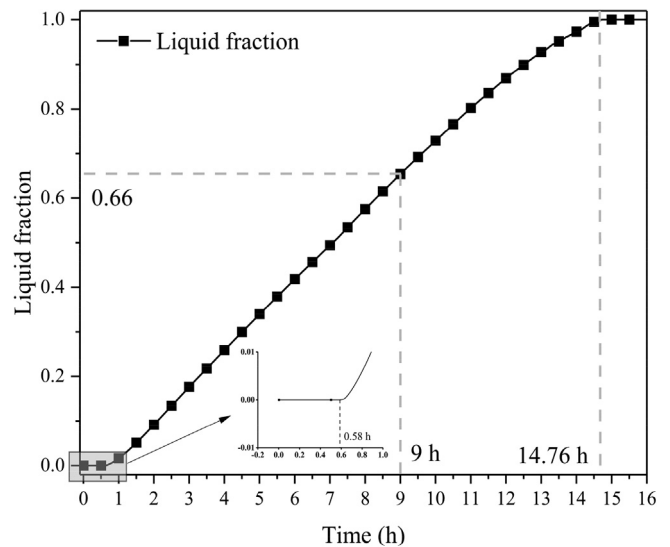

Fig. 8. Comparison of air temperature between experimental and simulation results.

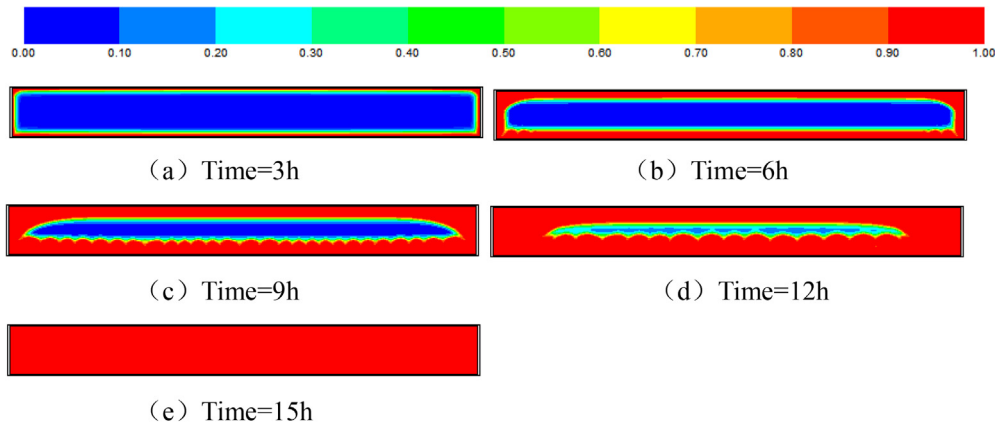**Fig. 9.** Liquid fraction as function of time.

Fig. 10. Instantaneous liquid fraction distribution at the vertical mid-plane of the PCM plate.
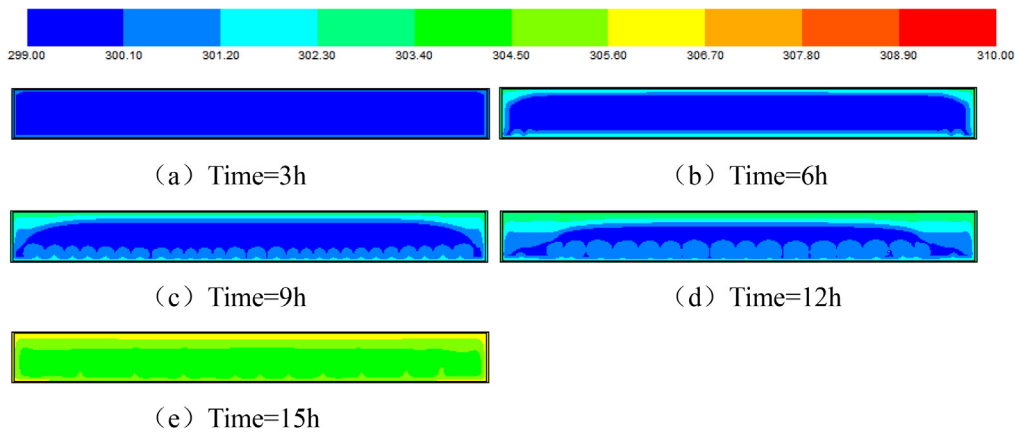

Fig. 11. Instantaneous temperature distribution at the vertical mid-plane of the PCM plate.
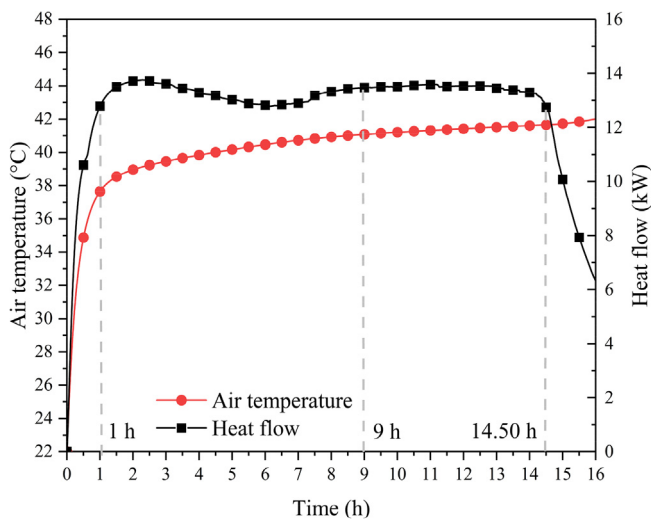

Fig. 12. Air temperature and heat flow of total PCM plates over time.

relationship between the air temperature and heat flow of the PCM plates; this relationship can be divided into three stages: (i) In the initial melting period (during the first hour), the PCM only melts slightly, and the air temperature rises sharply, from 22 °C to 37.64 °C. The PCM plates rapidly absorbs heat, and their heat flow increases from 0 to 12.77 kW. (ii) In the middle melting period (between 1 h and 14.50 h), the PCM continuously absorbs heat from

the air. The heat flow of total PCM plates maintains an average value of 13.34 kW. During this period, the majority of the heat is absorbed by the PCM, such that the air temperature rises slowly, increasing by 4.01 °C within 13.50 h. Additionally, at 9 h, the heat flow of total PCM plates is 13.48 kW, and the air temperature is 41.07 °C. (iii) In the late melting period (after 14.50 h), the PCM is about to melt completely, and relies mostly on sensible heat storage. Thus, the heat flow of total PCM plates decreases sharply, and the rise rate of the air temperature increases.

For the current operating conditions, the expected effect that the temperature should be maintained at 35 °C within 9 h is not satisfied. Therefore, it is necessary to analyze the influence factors, including the melting temperature, the latent heat, the thermal conductivity, and the size of the PCM plates. In addition, in order to facilitate the analysis, only one parameter should be changed and other parameters should be kept the same during the study.

5.1. Effect of melting temperature

The melting temperature of PCM is one of the most important parameters affecting the thermal properties of PCM plates. To investigate the effect of the melting temperature on the air temperature, the remaining parameters are kept constant. Thereafter, the melting temperature T_m is set to vary from 24 °C to 29 °C.

Figs. 13–15 show the liquid fraction of the PCM, the air temperature, and the temperature difference between the air and PCM for different melting temperatures, respectively. The results show that as the melting temperature increases, the melting rate of PCM
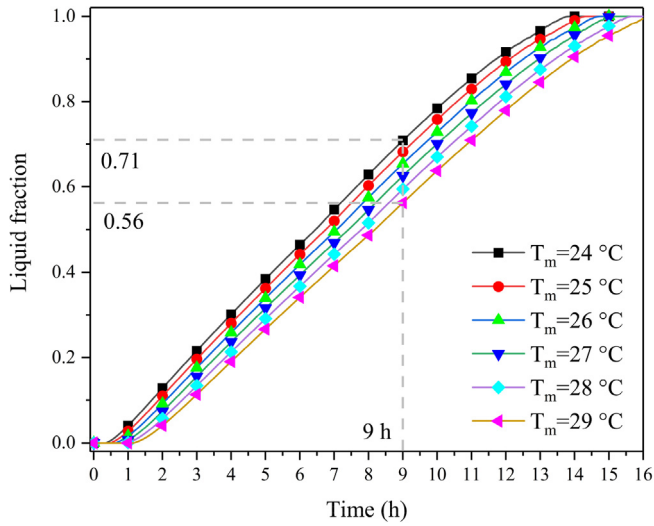
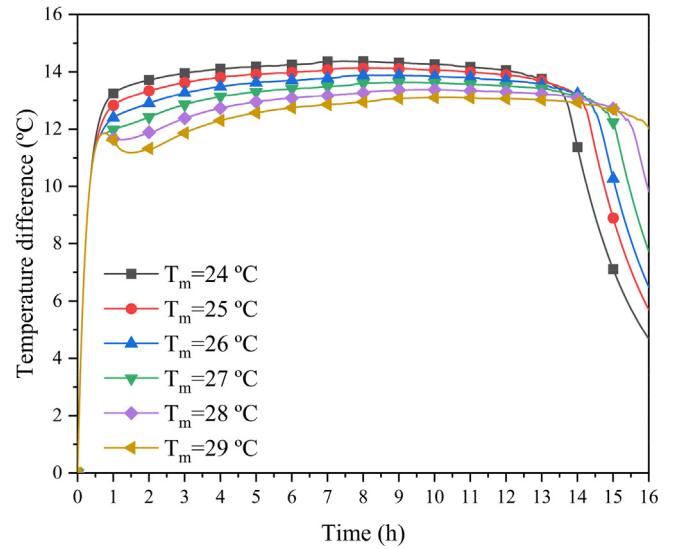**Fig. 13.** Liquid fraction curves at different melting temperatures.

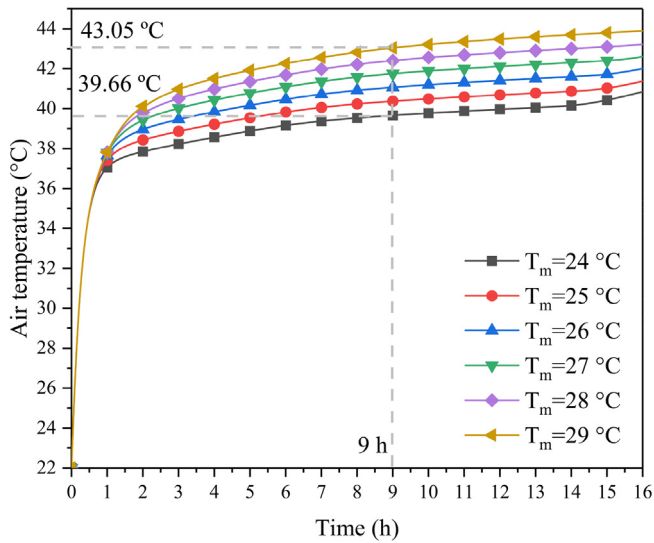**Fig. 14.** Air temperature curve at different melting temperatures.

Fig. 15. Temperature difference between air and PCM.

temperature increases by approximately 0.70 °C during the total melting time. This could be explained by the fact that temperature difference is the driving force for the transformation of PCM. As the melting temperature increases, the temperature difference between the indoor air and the PCM reduces, leading to the melting rate of PCM decreasing. Additionally, since the temperature of the information system room is normally maintained at 22–24 °C via the normal operation of air conditioning, PCM is not required to control the temperature of the information system room under normal circumstances (i.e. in the absence of power outages). Based on the above reasons and analysis, the melting temperature of the PCM should be 25 °C.

5.2. Effects of latent heat

The latent heat of the PCM also affects the thermal performance of the PCM plates. To investigate the influence of the latent heat on the air temperature control, the remaining parameters are kept constant. Accordingly, latent heat L is set to vary as 100, 120, 140, 160, 180, 200, and 220 kJ/kg.

Fig. 16. Liquid fraction curves at various latent heats.

equiproportionately decreases, and the air temperature isometrically rises. At the same time, the temperature difference between the air and the PCM decreases almost proportionally. Since the fully melted PCM relies on sensible heat absorption, it cannot maintain a state of approximate constant temperature, and the temperature rise rate is thus higher than the period in which it relies on latent heat absorption. Therefore, the temperature difference between the air and the PCM after completely melting decreases rapidly, and the occurrence time of the PCM with a melting temperature of 24 °C is earlier than that in other working conditions. When the melting temperature reaches 29 °C, the PCM does not completely melt at 16 h (as shown in Fig. 13), and the computed final liquid fraction is approximately 0.99. This leads to the slowness of the rise rate of the air temperature at 16 h. When the melting temperature of PCM is 24 °C and 29 °C, the liquid fraction of PCM is 0.71 and 0.56. With the increase in the melting temperature per 1 °C, the liquid fraction increases by 0.03, As can be seen in Fig. 14, compared with other working conditions, the air temperature is the lowest when the melting temperature of PCM is 24 °C, and the value is 39.66 °C at 9 h. Moreover, with the increase in the melting temperature per 1 °C, the average air

Fig. 16 shows the liquid fraction curves at various latent heats. It can be seen that liquid fraction of the PCM with different latent heats are all approximately 0.5 at 7 h. After 7 h, the higher the latent heat of the PCM, the slower the melting rate. However, before 7 h, this trend is reversed. Moreover, with the increase of latent heat, the time required for complete melting of the PCM increases. This can be attributed to the following: when the volume of a single PCM plate remains unchanged, the increase of latent heat improves the heat storage capacity of the single PCM plate, meaning that more heat and more time are required to melt the PCM completely.

Figs. 17 and 18 show the evolution of the heat flux of the PCM, and the heat flow of the total PCM plates over time, respectively, at seven different latent heats. With the increase of latent heat, the heat flux of the PCM increases, and the heat flow of total PCM plates shows a minor reduction. Due to the increase in the latent heat of the PCM, the melting time of the PCM is lengthened, such that the time needed for the efficient heat absorption of the PCM is increased. Thus, as can be seen in Fig. 17, the PCM with large latent heat has higher heat flux and longer heat absorption time than the PCM with small latent heat. For the whole information system room, the increase of latent heat leads to the reduction of the number of PCM plates and the total heat transfer area. Thus, for the case in which the heat storage capacity of the total PCM plates is constant, the heat flow of the total PCM plates decreases (as shown in Fig. 18). Additionally, in the middle and late melting period, the liquid fraction of the PCM with small latent heat is larger than that of the PCM with large latent heat, and there are fewer solid PCMs which do not melt. Therefore, at a certain time, the heat flow of total PCM plates with small latent heat decreases, while that of total PCM plates with large latent heat remains stable. Nonetheless, the overall value of the former is still large.

Fig. 19 shows the air temperature curves at various latent heats. It can be seen that the larger the latent heat, the higher the air temperature. Specifically, when the latent heat is 100 kJ/kg, the air temperature is 35.93 °C. With the increase in the latent heat per 20 kJ/kg, the average air temperature increases by approximately 1.20 °C during the total melting time. This can be attributed to the following: as can be seen Fig. 16, with the increase of latent heat of PCM, the melting time of PCM is prolonged, thus extending the time needed for the efficient heat absorption of the PCM. In the process of extension, the air temperature has been slowly rising.
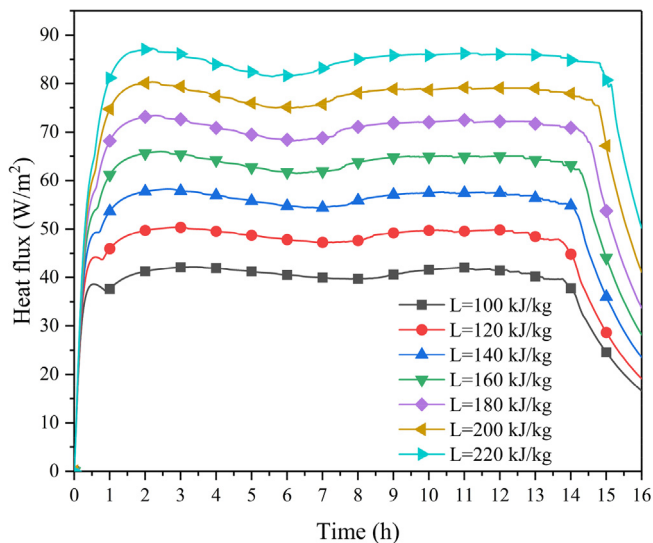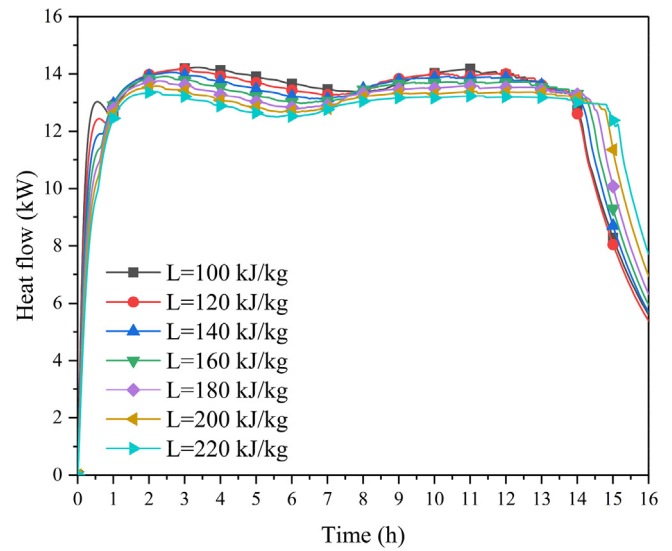

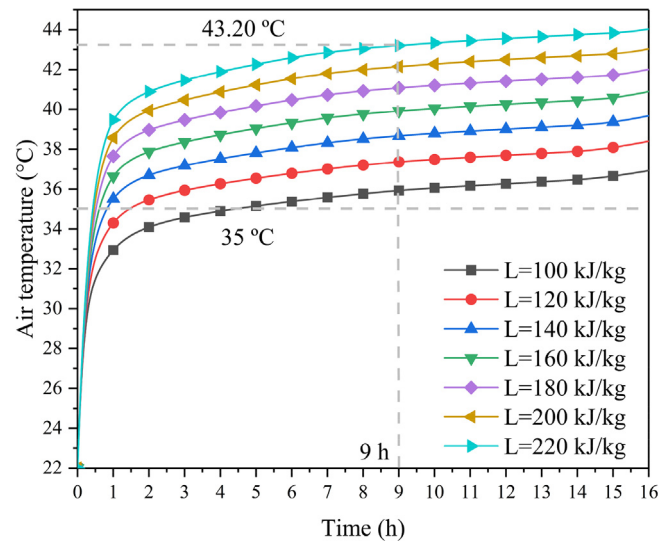**Fig. 18.** Heat flow of total PCM plates at various latent heats.

Fig. 19. Air temperature curves at various latent heats.

Therefore, the higher the latent heat, the higher the air temperature.

5.3. Effects of thermal conductivity

Enhancing the thermal conductivity of the PCM is a research objective of many scholars, which indicates its importance to the heat transfer performance of PCM. To investigate the influence of the thermal conductivity of PCM on air temperature control and find a suitable thermal conductivity value, the remaining parameters are kept constant. Accordingly, the thermal conductivity k is set to vary as 0.2, 0.6, 1.0, 1.4, and 1.8 W/(m·K).

Figs. 20–22 show the changes in the liquid fraction of the PCM, the heat flow of the total PCM plates, and the air temperature for different thermal conductivities, respectively. The results show that as the thermal conductivity increases, the melting rate and heat flow of the PCM shows minor growth. With the increase in the thermal conductivity of the PCM, the melting time of the PCM is shortened, such that the time needed for the efficient heat absorption of the PCM is reduced. It is also found that increasing

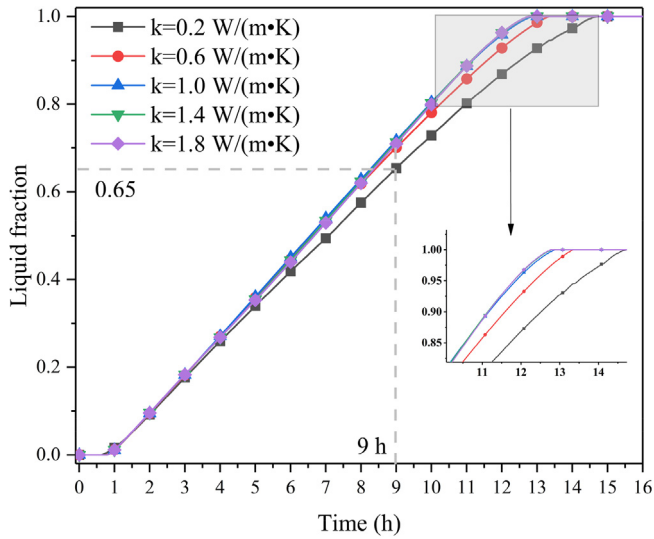**Fig. 17.** PCM heat flux at various latent heats.

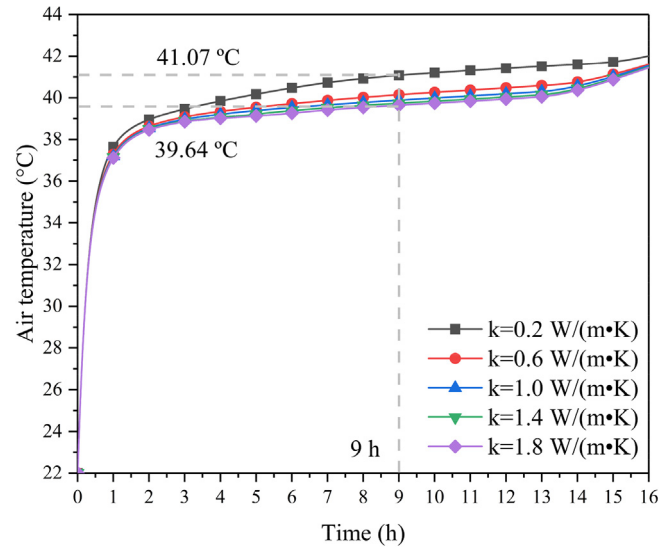Fig. 20. Liquid fraction curves at different thermal conductivities.

Fig. 22. Air temperature curves at different thermal conductivities.
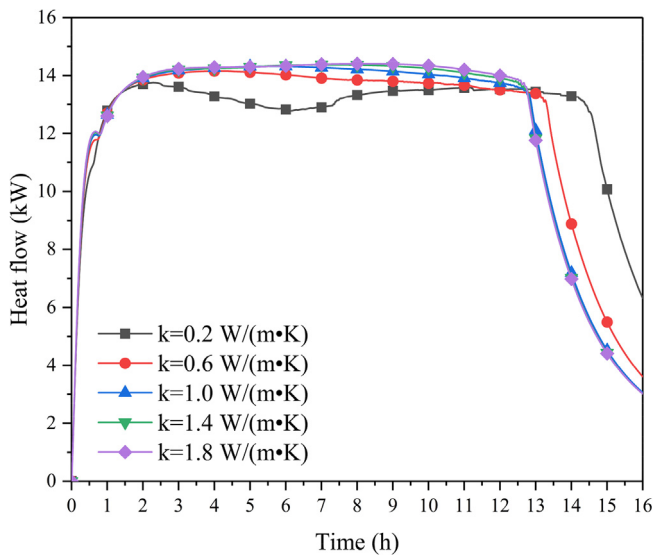

Fig. 21. Heat flow of total PCM plates at different thermal conductivities.

the thermal conductivity of the PCM can reduce the temperature as well as shorten the temperature control time. It can be seen from Fig. 21 that the larger the thermal conductivity, the smaller the fluctuation in the PCM heat flow. This could be attributed to the fact that the thermal conductivity has a direct influence on the internal heat transfer of the PCM plate. The ascension of thermal conductivity can lead to a reduction of the internal thermal resistance, and enhancement of the heat transfer inside the PCM plate. However, as the thermal conductivity approaches 1 W/(m·K), further increases in the thermal conductivity have no marked impact on the heat transfer effect of the PCM. When the thermal conductivity is 0.2 W/(m·K) and 0.6 W/(m·K), the air temperature is 41.07 °C and 40.14 °C. The change of air temperature under other working conditions is less than 0.1. The results in the Figs. 20–22 clearly show that when the thermal conductivity is 1.0, 1.4, and 1.8 W/(m·K), the curves are almost identical. The reason for this is as follows: the external thermal resistance of the PCM plate is stable with the variation of the thermal conductivity of the PCM. Therefore, as the thermal conductivity approaches 1 W/(m·K), further increases in the thermal conductivity have no marked impact on the melting rate and heat flow of the PCM.

5.4. Effect of the size of the PCM plates

Even with the same volume, different unit sizes show different influences on the heat transfer and melting processes. To investigate the effect of the size of the PCM plates on the air temperature, the remaining parameters are kept constant. Under the operating conditions studied herein, four sizes are investigated. The relevant parameters regarding the four sizes of the PCM plates are shown in Table 3.
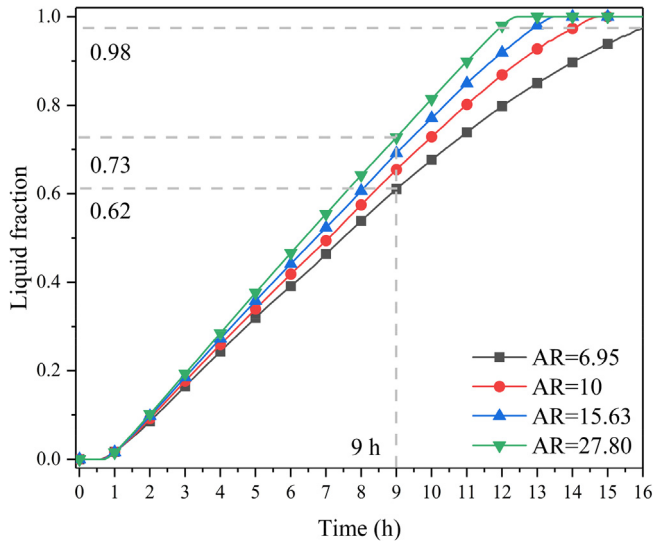
Fig. 23 presents the liquid fraction curves for different sizes of PCM plates. It is noted that with the increase of the aspect ratio of the PCM plates, the melting rate of the PCM is accelerated, but the effect is gradually reduced. Compared with other working conditions, the liquid fraction is the biggest when the aspect ratio of the PCM plates is 27.80, and the value is 0.73 at 9 h. When the aspect ratio of the PCM plates is 6.95, the result shows that the PCM does not completely melt: the computed final liquid fraction is approximately 0.98. This could be attributed to the following: under the condition of constant volume, the increase of the aspect ratio of the PCM plates means that the specific surface area of the PCM enlarges. However, with the gradual increase of the aspect ratio of the PCM plates, the increasing trend of surface area gradually decreases, such that the change in the melting rate decreases.

Figs. 24 and 25 present the evolution of heat flux of the PCM and heat flow of the total PCM plates over time, respectively, at different sizes of PCM plates. The results show that as the aspect ratio of the PCM plates increases, the PCM heat flux reduces and the heat flow of the total PCM plates increases. The is attributed to the following: according to Newton's cooling formula $Q = hA(T_f - T)$, the larger the specific surface area of the PCM plates, the more heat they can absorb, and the heat flow of total PCM plates is accelerated. However, the latent heat of the single PCM plate remains unchanged, such that the heat required for PCM melting remains constant. Therefore, as the surface area of the PCM plate increases, the PCM heat flux decreases. Additionally, in the middle and late period, the heat flux of the PCM with a large aspect ratio decreases, while that of the PCM with a small aspect ratio simultaneously remains stable. The reason for this is as follows: as the aspect ratio of the PCM plates increases, the melting rate of the PCM increases and the melting time of the PCM is shortened. Therefore, the time needed for the efficient heat absorption of the PCM is reduced.

Fig. 26 illustrates the variation of the air temperature over time at five different aspect ratios. It is found that increasing
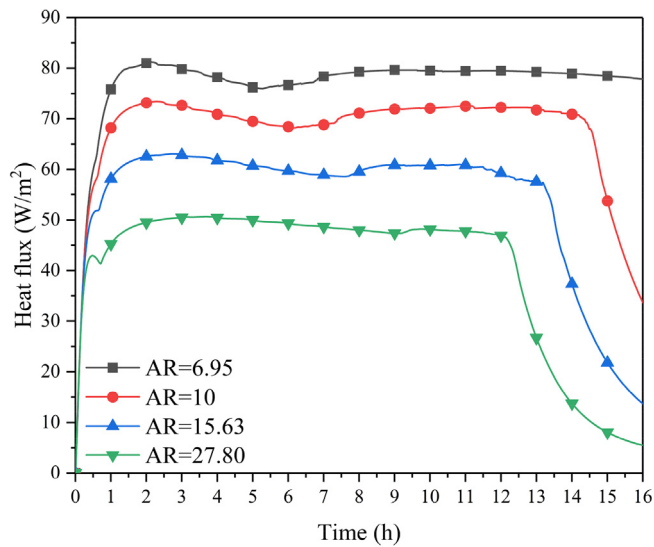
Table 3
Four sizes of PCM plates.

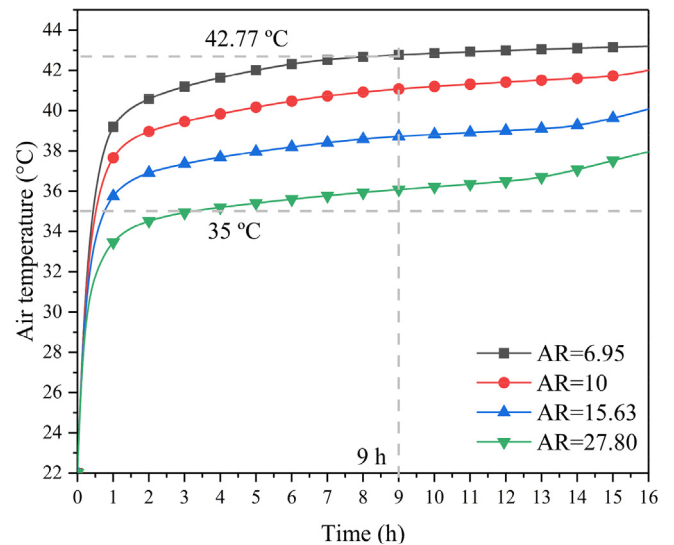| Condition	Length (mm)	Width (mm)	Height (mm)	Surface area of a PCM plate (m^2)	Aspect ratio (AR; equal to width/height)
1	600	417	60	0.62	6.95
2	600	500	50	0.71	10
3	600	625	40	0.85	15.63
4	600	834	30	1.09	27.80

Fig. 23. Liquid fraction curves at different sizes of PCM plates.
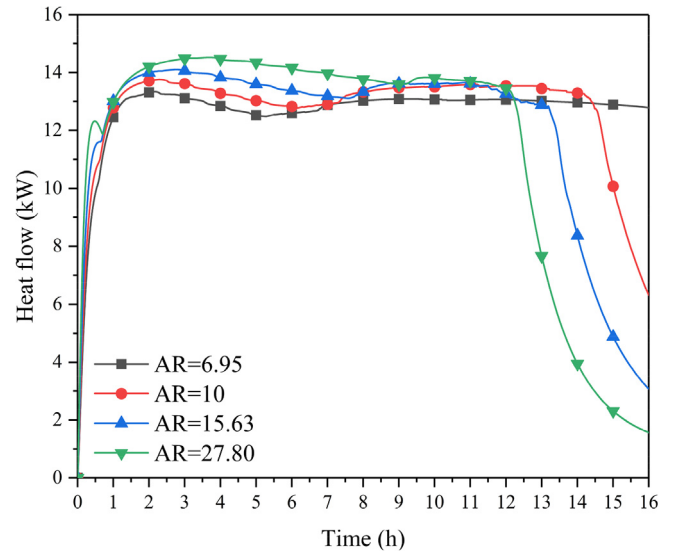
Fig. 25. Heat flow of total PCM plates at different sizes of PCM plates.

Fig. 24. PCM heat flux at different sizes of PCM plates.

Fig. 26. Air temperature curve at different sizes of PCM plates.

5.5. Parameter optimization

Based on the above analyses and discussions, the values of the melting temperature, latent heat, thermal conductivity, and size of the PCM plates are selected as 25 °C, 120 kJ/kg, 1 W/(m·K), and 600 mm × 834 mm × 30 mm, respectively. Thereafter, to investigate these parameters' suitability in satisfying the expected requirements, calculation analysis was conducted as follows.

Comparing Fig. 27 with Fig. 9, it can be concluded that the PCM melting rate is accelerated after parameter optimization. Compared to Fig. 12, the heat flow of the total PCM plates from

the aspect ratio of PCM plates can not only reduce the air temperature, but also shorten the temperature control time. Specifically, as the aspect ratio of PCM plate increases from 6.95 to 27.80, the air temperature varies as 42.77 °C, 41.07 °C, 38.71 °C, and 36.08 °C at 9 h. This is because, the higher the aspect ratio of the PCM plates, the larger heat flow of the total PCM plates. Additionally, when the aspect ratio of the PCM plates is 6.95, an incomplete melt of the PCM leads to a slow rise rate of the air temperature at 16 h.
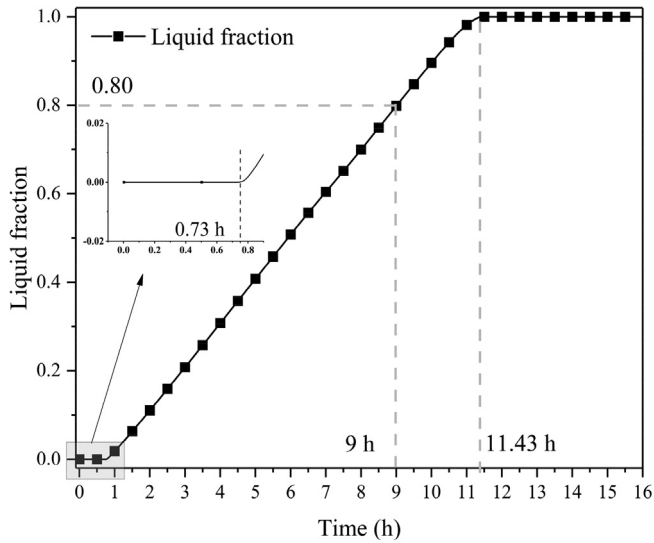
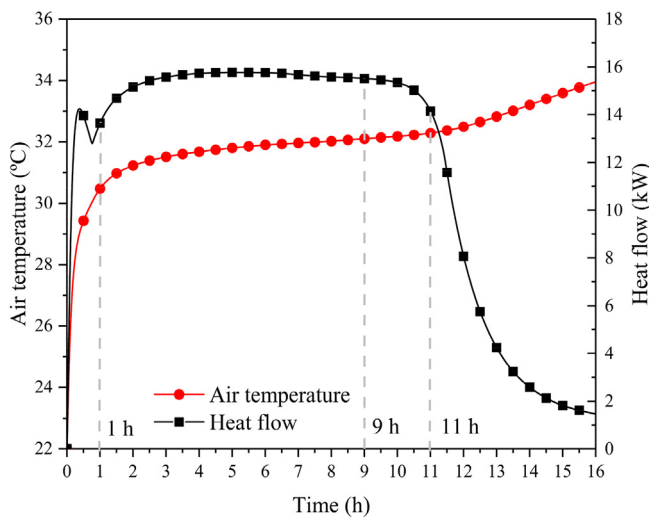**Fig. 27.** Liquid fraction curves of optimized PCM plates.

Fig. 28. Heat flow and air temperature curves of optimized PCM plates.

Fig. 28 increases, and the air temperature is significantly reduced. Specifically, in the initial melting period (in the first hour), the heat flow of the total PCM plates and the air temperature rise rapidly. At 0.73 h, the PCM begins to melt, and the heat flow fluctuates. At 1 h, the heat flow of the total PCM plates is 13.63 kW, and the air temperature is 30.47 °C. In the middle melting period (between 1 h and 11 h), the heat flow of the total PCM plates is stable, at approximately 15.44 kW, and the air temperature increases slowly. From 1 h to 11 h, the air temperature only increases by 1.63 °C. At 9 h, the liquid fraction of the PCM and the air temperature is 0.80 and 32.10 °C, respectively. The liquid fraction of the PCM is approximately 0.98 at 11 h. In the late melting period (after 11 h), the rise rate of air temperature significantly increases, because the PCM is about to melt completely. The PCM is completely melted at 11.47 h. At 16 h, the air temperature is 33.96 °C. As the objective of this study is to demonstrate the cooling system utilizing the PCM plates that can maintain the information system room temperature below 35 °C during an emergency power failure, the optimized operating condition successfully fulfills the study objective.

6. Conclusion

This study takes an information system room under the condition of an emergency power failure as the research object. By employing a cooling system that implements PCM plates, the feasibility of temperature control in this intensive heat-releasing space are demonstrated. For the cooling system of an information system room, a mathematical heat transfer model, which considers the air, heat source, phase change cooling devices, and enclosure structure of the room, was established. The performance of the PCM and air temperature were analyzed. Then, the effects of some impact factors, such as the melting temperature, latent heat, thermal conductivity, size of the PCM plates, were investigated. The conclusions from these analyses and investigations are summarized as follows:

1) Under the condition of parameter optimization, the air temperature is 32.10 °C at 9 h. Therefore, the cooling system utilizing the PCM plates can effectively maintain the temperature of the information system room below 35 °C within 9 h. Until 16 h, the air temperature remains below 35 °C.
2) The temperature control process of the PCM can be divided into three stages. In the initial and late melting period, the PCM relies mostly on sensible heat storage. Thus, both the air temperature and heat flow of the total PCM plates rise sharply. In the middle melting period, the heat flow of the total PCM plates is stable, and the air temperature rises slowly.
3) Increasing the aspect ratio of PCM plates and decreasing PCM latent heat have the similar effect on the air temperature control. Additionally, the two parameters are related to the surface area of the PCM plates.
4) The lower the melting temperature of the PCM, the better the air temperature can be controlled. For the conditions considered in this study, the appropriate melting temperature is approximately 25 °C.
5) With the increase of the thermal conductivity, the air temperature reduces, and the fluctuation of the PCM heat flow significantly decreases. However, as the thermal conductivity approaches 1 W/(m·K), further increases in the thermal conductivity have no marked impact on the air temperature control.

Here, the heat transfer rate of PCM is largely limited by natural convection. Therefore, small mechanical energy storage devices should be integrated to achieve forced convection and further optimize the temperature control effect. Additionally, as no experiment is conducted herein, subsequent experiments should be carried out.

CRediT authorship contribution statement

Jing Wang: Methodology, Software, Formal analysis, Writing - original draft. **Xiaoling Cao:** Conceptualization, Writing - review & editing, Data curation, Project administration. **Yanping Yuan:** Resources, Supervision, Funding acquisition. **Ziyu Leng:** Investigation, Data curation. **Yafen Sun:** . **:** Validation.

Declaration of Competing Interest

The authors declare that they have no known competing financial interests or personal relationships that could have appeared to influence the work reported in this paper.

Acknowledgements

References

[1] Q/CR571-2017, Technical specification of railway information system room.
[2] J. Hou, Z. Yang, P. Xu, G. Huang, Design and performance evaluation of novel personal cooling garment, Appl. Therm. Eng. 154 (2019) 131–139.
[3] T.Y. Kim, B.S. Hyun, J.J. Lee, J. Rhee, Numerical study of the spacecraft thermal control hardware combining solid-liquid phase change material and a heat pipe, Aerosp. Sci. Technol. 27 (2013) 10–16.
[4] A. Arshad, H.M. Ali, M. Ali, S. Manzoor, Thermal performance of phase change material (PCM) based pin-finned heat sinks for electronics devices: Effect of pin thickness and PCM volume fraction, Appl. Therm. Eng. 112 (2017) 143–155.
[5] W. Wu, N. Liu, W. Cheng, Y. Liu, Study on the effect of shape-stabilized phase change materials on spacecraft thermal control in extreme thermal environment, Energy Convers. Manage. 69 (2013) 174–180.
[6] A. Maiorino, M. Gesù Del Duca, A. Mota-Babiloni, A. Greco, C. Aprea, The thermal performances of a refrigerator incorporating a phase change material, Int. J. Refrig 100 (2019) 255–264.
[7] M.I. Hasan, H.O. Basher, A.O. Shdhan, Experimental investigation of phase change materials for insulation of residential buildings, Sustainable Cities and Society. 36 (2018) 42–58.
[8] H.B. Kim, M. Mae, Y. Choi, Application of shape-stabilized phase-change material sheets as thermal energy storage to reduce heating load in Japanese climate, Build. Environ. S0360132317303918 (2017).
[9] F. Souayfane, P.H. Biwole, F. Fardoun, P. Achard, Energy performance and economic analysis of a TIM-PCM wall under different climates, Energy. 169 (2019) 1274–1291.
[10] D. Li, Y. Zheng, C. Liu, et al., Numerical analysis on thermal performance of roof contained PCM of a single residential building, Energy Convers. Manage. 100 (2015) 147–156.
[11] S. Valizadeh, M. Ehsani, M.T. Angji, Development and thermal performance of wood HPDE- PCM nanocapsule floor for passive cooling in building, Energy Sources Part A 41 (2019) 2114–2127.
[12] M. Alizadeh, S.M. Sadrameli, Indoor thermal comfort assessment using PCM based storage system integrated with ceiling fan ventilation: Experimental design and response surface approach, Energy Build. 188 (2019) 297–313.
[13] X. Chen, Q. Zhang, Z.J. Zhai, X. Ma, Potential of ventilation systems with thermal energy storage using PCMs applied to air conditioned buildings, Renewable Energy 138 (2019) 39–53.
[14] S. Baek, S. Kim, Analysis of Thermal Performance and Energy Saving Potential by PCM Radiant Floor Heating System based on Wet Construction Method and Hot Water, Energies. 12 (2019), https://doi.org/10.3390/en12050828.
[15] N. Chaiyat, T. Kiatsiriroat, Energy reduction of building air-conditioner with phase change material in Thailand, Case Studies in Thermal Engineering. 4 (2014) 175–186.
[16] Y. Yuan, X. Gao, H. Wu, et al., Coupled cooling method and application of latent heat thermal energy storage combined with pre-cooling of envelope: Method and model development, Energy. 119 (2017) 817–833.
[17] X. Gao, Y. Yuan, X. Cao, et al., Coupled cooling method and application of latent heat thermal energy storage combined with pre-cooling of envelope: Sensitivity analysis and optimization, Process Saf. Environ. Prot. 107 (2017) 438–453.
[18] M. Zhang, Q. An, Z. Long, W. Pan, H. Zhang, X. Cheng, Optimization of Airflow Organization for a Small-scale Date Center Based on the Cold Aisle Closure, Procedia Eng. 205 (2017) 1893–1900.
[19] S. Hoseinzadeh, R. Ghasemiasl, D. Havaei, A.J. Chamkha, Numerical investigation of rectangular thermal energy storage units with multiple phase change materials, J. Mol. Liq. 271 (2018) 655–660.
[20] J. Vogel, J. Felbinger, M. Johnson, Natural convection in high temperature flat plate latent heat thermal energy storage systems, Appl. Energy 184 (2016) 184–196.
[21] Rubitherm. PCM RT-LINE, http://www.rubitherm.eu/en/index.php/productcategory/organische-pcm-rt/; 2019 [accessed 15 September 2019].
[22] L. Cheng, J. Yajing, S. Tiantian, Study on Influences of Building Envelope Insulation Performance on Energy Consumption of Air-conditioning System for Communication Buildings, Build. Sci. 28 (10) (2012) 68–72.
[23] C. Chongwen, N. Yougang, Air conditioning design of machine room, China Architecture & Building Press (1995).
[24] Lu Yaoqing, Practical heating and air conditioning design manual, China Architecture & Building Press (1993).
[25] A.D. Brent, V.R. Voller, K.J. Reid, Enthalpy-porosity technique for modeling convection-diffusion phase change: application to the melting of a pure metal, Numer. Heat Transf. 13 (1988) 297–318.
[26] V.R. Voller, C. Prakash, A fixed grid numerical modelling methodology for convection-diffusion mushy region phase-change problems, Int. J. Heat Mass Transf. 30 (1987) 1709–1719.
[27] A.C. Kheirabadi, D. Groulx, The effect of the mushy-zone constant on simulated phase change heat transfer, Rutgers University, New Brunswick, NJ, USA, 2015, pp. 528–549.
[28] W.-B. Ye, Thermal and hydraulic performance of natural convection in a rectangular storage cavity, Appl. Therm. Eng. 93 (2016) 1114–1123.
[29] C. Xiaoling, Y. Yuan, Numerical investigation on optimal number of longitudinal fins in horizontal annular phase-change unit at different wall temperatures, Energy Build. 158 (2018) 384–392.
[30] A. Abdi, V. Martin, J.N.W. Chiu, Numerical investigation of melting in a cavity with vertically oriented fins, Appl. Energy 235 (2019) 1027–1040.
[31] Z. Ximin, Z. Tong, et al., Heat Transfer, 6th ed., China Architecture & Building Press, 2014.
[32] J. Vogela, A. Thess, Validation of a numerical model with a benchmark experiment for melting governed by natural convection in latent thermal energy storage, Appl. Therm. Eng. 148 (2019) 147–159.
[33] P. Jany, A. Bejan, Scaling theory of melting with natural convection in an enclosure, Int. J. Heat Mass Transf. 31 (1988) 1221–1235.
[34] R. Karami, B. Kamkari, Investigation of the effect of inclination angle on the melting enhancement of phase change material in finned latent heat thermal storage units, Appl. Therm. Eng. 146 (2019) 45–60.
[35] B. Wu, B. Lei, C. Zhou, et al., Experimental study of phase change material's application in refuge chamber of coal mine, Procedia Eng. 45 (2012) 936–941.
[36] B. Kamkari, D. Groulx, Experimental investigation of melting behaviour of phase change material in finned rectangular enclosures under different inclination angles[J], Exp Therm Fluid Sci. 97 (2018) 94–108.
[37] F.L. Tan, S.F. Hosseinizadeh, J.M. Khodadadi, Liwu Fan, Experimental and computational study of constrained melting of phase change materials (PCM) inside a spherical capsule, Int. J. Heat Mass Transf. 52 (2009) 3464–3472.